 Proceedings of ICCES'08, pp.891-896

Patient Specific Knee Joint Finite Element Model Validation with High Accuracy Kinematics from Biplane Dynamic Radiography

G. Papaioannou[1], G. Nianios[1], C. Mitroyiannis[1], S.Tashman[2], K.H. Yang[2]

Summary

Little is known about in vivo menisci loads and displacements in the knee during strenuous activities. We have developed a method that combines biplane high-speed dynamic radiography (DRSA) and a subject-specific finite element model for studying in vivo meniscal behavior. In a very controlled uniaxial compression loading condition, removing of the pressure sensor from the model can result in relatively large errors in contact and cartilage stress that are not reflected in the change of meniscal displacement.

Introduction

Hypotheses have been put forth that the degeneration caused by osteoarthritis is initiated through mechanical loading [1-7]. Knee ligament injuries and other aspects of knee mechanics are known to influence the development and progression of osteoarthritis (OA). In spite of this large body of evidence supporting the link between mechanical factors and OA, the specific mechanistic nature of damaging in-vivo joint kinematics/loads remains elusive. An understanding of mechanical factors in OA pathogenesis requires knowledge of the joint contact mechanics. The complexity of these problems requires implementation of sophisticated numerical methods for solutions. The present study proposes a new FE approach ideally suited for obtaining solutions for knee joint contact problems.

Methods

A single left knee from a cadaveric specimen (male, age 31yrs) was prepared for placement in a uniaxial load application system. Tantalum beads (0.8mm) were placed along the line of anterior cruciate ligament, (n=7), the menisci (n=18), the tibia (n=3) and femur (n=3). For this task an arthroscopic procedure was employed so that soft tissues and joint capsule remained intact. Specimens were fixed in cups, aligned with the load application system at 10 degrees flexion and placed within the biplane radiography system (Figure 1).

The in-situ 3D kinematics of all tantalum beads was measured using DRSA at 250 frames/s (dynamic accuracy $\pm$0.1mm [4]). Meniscal kinematics and knee motion were assessed during a series of uniaxial compressive loading protocols (0-1kN at a rate of 10-500mms^{-1}). A K-scan pressure sensor (Tekscan Corporation,

[1]Human Movement Sciences, Bioimaging and Advanced Biomechanics Laboratory, University of Wisconsin Milwaukee, Milwaukee, WI, USA

[2]Bioengineering Center, Wayne State University, Detroit MI, USA

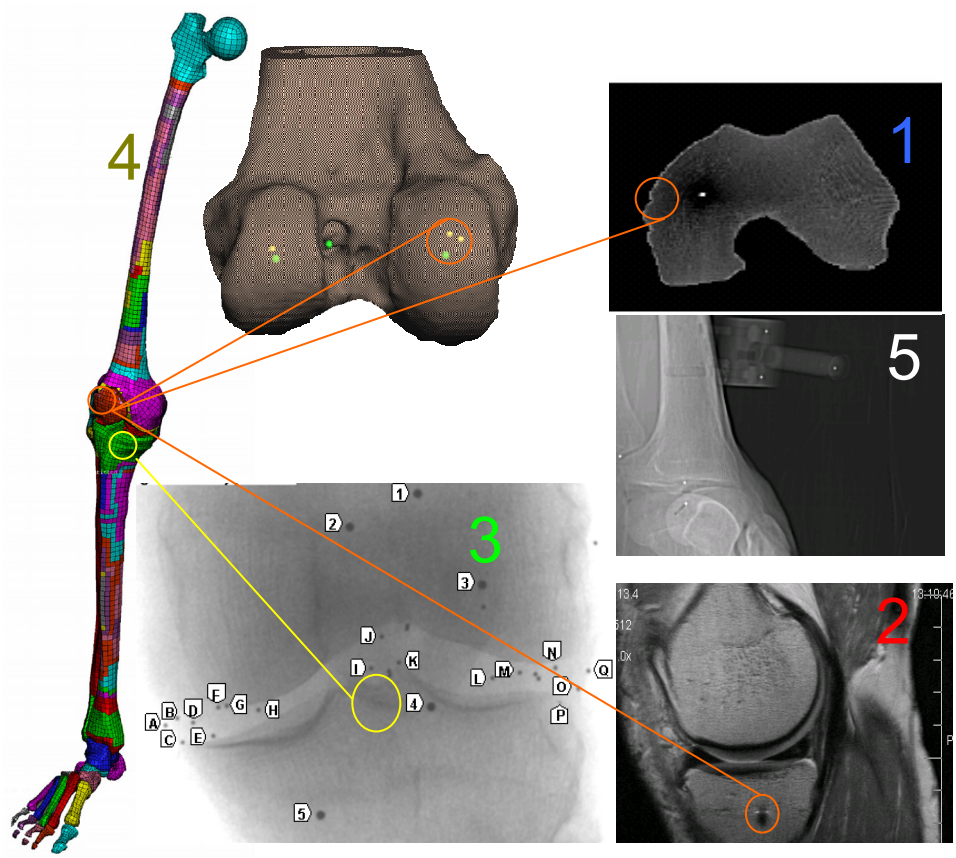

Figure 1: Image fusion process to deliver higher mesh density and patient specificity in the development of the solid model:1) Computed tomography data 2) MRI data 3) Image from menisci and Anterior cruciate ligament with tantalum beads from the DRSA system, 4) The Whole Lower limb FE model and the reconstructed femur bone surface data, 5) Note the presence of tantalum markers in all imaging modalities for co-registration (Cupric Sulfate tube).

S.Boston, MA) was then fixed to the tibia plateaus using an arthroscopic procedure. The loading protocol was repeated to evaluate the effect of the sensor on the pressure distribution profile. To construct the model a CT (GE) system was used to scan the knee in 0.5 mm increments. Two plastic tubes filled with solution of Cupric Sulfate with paramagnetic properties were fixed in the femur and tibia prior to magnetic resonance imaging (MRI) for tantalum based co-registration (Figure 1(5)). MRI (GE 3 T system) scans included coronal T2, sagittal proton density weighted imaging using a fast spin echo sequence and sagittal spoiled gradient echo imaging. Fusion of imaging protocols allowed for geometry description

of meniscal and articular cartilage. The model steams from a previously published work of Wayne State University that includes the whole lower extremity [2][4]. The model was modified to reflect the geometry information of the cadaveric high resolution volumetric data. This resulted in two mesh densities at the tibiofemoral contact area: original (where element thickness averaged 7mm for bone and 4mm for cartilage) and high mesh density (2 and 1 mm respectively). Solid eight-node elements were used throughout the contact surfaces. Cartilage was modeled using an elastic material law. The constitutive relation of the menisci treated the tissue as transversely isotropic and linearly elastic. The surface-to-surface tangential contact algorithm (ABAQUS-HKS Inc., Pawtucket, RI) was applied for the surface interaction. Boundary conditions for the calculation were determined from the high accuracy skeletal and meniscal DRSA kinematics and the loads on the femur (from a 6-axis load cell at the proximal femur interface) (Figure 2). During compressive loading(1500N), all three rigid-body translations and rotations of the proximal tibia were prescribed using the 3D displacements of the bone tantalum beads, whereas the distal femur was fully constrained (Flexion/Extension). Convergence of the equilibrium iteration was assessed based on two independent criteria. In the first, the maximum residual nodal force was required to be less than a user-defined fraction of a spatially and temporally averaged force for the entire structure (0.8%). In the second, the last iterative correction to the incremental nodal displacement was required to be less than 1% of the incremental nodal displacement itself at each node. To check for model convergence, the contact variables were recorded for the two mesh sizes.

Results

The convergence test indicated improved finite element solution for mesh size of 1 mm by 1 mm. Increasing the mesh to the large mesh size of 4 mm by 4 mm changed all but one of the contact variables by up to 45% (Table 1). The load was applied in 10 increments and contact was the primary source of nonlinearity in the problem. The total force due to contact increased on the lateral side by 9%. This was mirrored by a decrease in total contact force on the medial side by 7.4%.

The location of the center of pressure shifted slightly medioposteriorly on the medial tibial plateau. In the medial side, the largest shifts of 0.5 mm in the medial direction and 0.3 mm in the posterior direction occurred with the small sized mesh. Differences in contact variables as large as 14% occurred when the k-scan sensor was excluded from the FE model. The largest difference was in the maximum pressure (increase of 18%). The model predicted most of the contact variables (on average an RMS error of 0.91) measured experimentally with the Tekscan pressure sensor (Figure 2). We were able to track meniscal radial displacement based on the menisci tantalum beads and use it to evaluate the deformation of menisci.

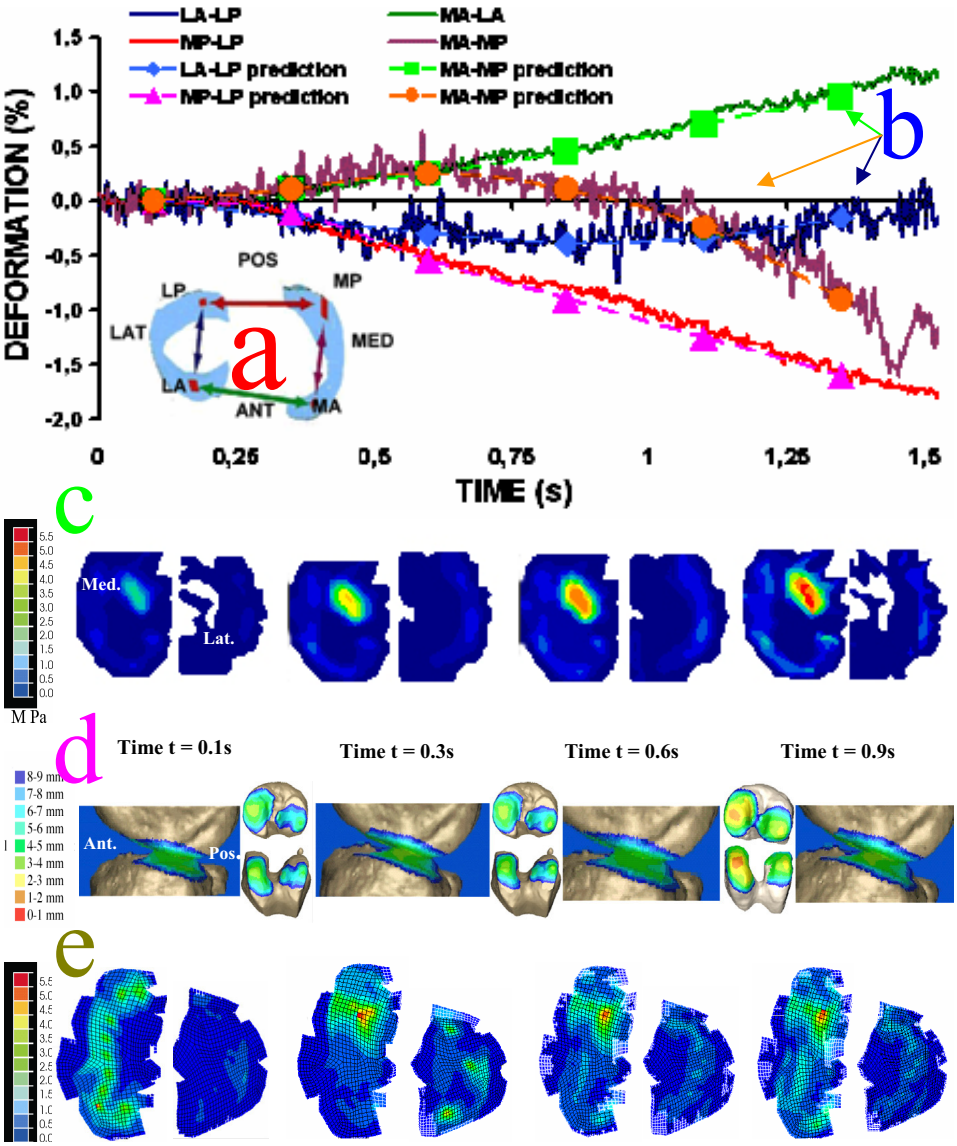

Figure 2: a) Deformation between meniscal markers and model predictions during compressive force of 1500 N applied through the distal tibia at 10 degrees of flexion. (corresponding closest element node motion): MA: Medial anterior, MP medial-posterior,LP lateral posterior, LA lateral anterior, b) the model convergence points are shown in circles and the FE predictions in dashed lines, c)The history of contract pressure in the first second of load application up to the max load as recorded by the Tekscan sensor, d) Euclidian distance (proximity map) between the tibia and femur during the loading phase e) FE calculation of contact pressure at the tibia plateau.

Table 1: The effect of mesh density on contact variables. Fast (number on top) and slow (number on bottom) rate loading for the 1500N maximum compression example.

Average Element Size	Peak Pressure (MPa)		Mean Pressure (MPa)		Total Force (N)		Area (mm^2)	
	LAT	MED	LAT	MED	LAT	MED	LAT	MED
4 x 4 mm	3.91	5.71	1.27	2.12	390	590	386	440
	2.87	4.4	0.67	1.01	290	500	345	490
1 x 1 mm	3.26	4.72	0.78	1.98	310	508	443	490
	2.61	2.62	0.54	1.24	210	460	470	535

Discussion

The study permitted acquisition of the menisci kinematics, estimations of menisci radial expansion and direct measurement of articular pressure in the different loading sequences. Motion between the medial and lateral menisci was greater than displacement within the meniscal bodies, reaching a peak of approximately 1.5%. The gross radial medial-lateral and anterior-posterior meniscal displacement due to pure joint compression of 1 kN was comparable to the predicted model deformations (figure 2). Insertion of the Tekscan sensor had a minimal effect ($<$2%) on measured marker displacements. The FE solution was considered converged for an average element size of 1.5 mm by 1.5 mm. The FE predicted contact force of 550 N in the medial and 320 N in the lateral tibial condyle. Using this mesh size, finite element solutions for the meniscus, indicated that the contact variables changed by more than 7% when we introduced the Tekscan in the FE model. The model was validated using high accuracy 3D kinematics of markers placed directly in the menisci. Good agreement between model predictions and experimental measurement was found. We concluded that even in a very controlled uniaxial compression loading condition exclusion of the K-scan sensor from the model can result in relatively large errors in contact and cartilage stress that are not reflected in the change in meniscal kinematics. This local validation enhances the fidelity of the FE knee model and its applicability in the study of articular stress.

References

1. Beillas P., Begeman, P. C., Yang, K. H., King, A. I., Arnoux, P.-J., Kang, H.-S., Kayvantash, K., Brunet, C., Cavallero, C. and Prasad, P., 2001. Lower Limb: Advanced FE Model and New Experimental Data. *Stapp Car Crash J.* 45: 469-94.

2. Beillas P., Papaioannou G., Tashman S., Yang K. 2004. A New method to investigate *in-vivo* Knee behavior using a Finite Element Model of the Lower Limb. *J. Biomech* 37: 1019-30.

3. Donahue T. L. H., Hull M. L., Rashid M. M., Jacobs C. R. 2003. How the stiffness of meniscal attachments and meniscal material properties affect tibio-femoral contact pressure computed using a validated finite element model of the human knee joint. *Journal of Biomech* 36: 19-34.

4. Donzelli P. S., Spilker R. L., Ateshian G. A., Mow V. C. 1999. Contact analysis of biphasic transversely isotropic cartilage layers and correlations with tissue failure. *J Biomech* 32: 1037-47.

5. Keyak J. H., Skinner H. B. 1992. Three-dimensional finite element modelling of bone: effects of element size. *J Biomed Eng* 14: 483-9.

6. Papaioannou G., Guettler J., Jurist K., Fyhrie D., Tashman S., Yang K. H. 2004. FE Modelling of the Osteochondral Defects in the Human Knee: Influence of Defect Size on Cartilage Rim Stress and Load Redistribution to Adjacent Cartilage. In *Scattering Theory and Biomedical Engineering Modeling and Applications*, ed. G.Dassios, K. Kiriaki, C.V. Massalas: World Scientific.

7. Papaioannou G., Tashman S., Fyhrie D., Knight R., Yang K. H. 2003. Menisci Radial Displacement under Joint Load. In *Scattering Theory and Biomedical Engineering Modelling and Applications*, ed. G. Dassios, K. Kiriaki, C.V. Massalas: World Scientific.